An unexpected and persistent increase in global emissions of ozone-depleting CFC-11

Stephen A. Montzka [1]*, Geoff S. Dutton[1,2], Pengfei Yu[1,2], Eric Ray[1,2], Robert W. Portmann[1], John S. Daniel[1], Lambert Kuijpers[3], Brad D. Hall[1], Debra Mondeel[1,2], Carolina Siso[1,2], David J. Nance[1,2], Matt Rigby[4], Alistair J. Manning[5], Lei Hu[1,2], Fred Moore[1,2], Ben R. Miller[1,2], James W. Elkins[1].

The Montreal Protocol was designed to protect the stratospheric ozone layer by reducing the abundance of ozone-depleting substances such as chlorofluorocarbons (CFCs) in the atmosphere[1,2,3]. The reduction in atmospheric concentration of trichlorofluoromethane (CFC-11) has made the second largest contribution to the decline in the total atmospheric concentration of ozone-depleting chlorine since the 1990s [1]. However, CFC-11 still contributes one-quarter of all chlorine reaching the stratosphere and a timely recovery of the stratospheric ozone layer depends on the sustained decline in CFC-11 concentrations[1]. Here we show that the rate of decline in atmospheric CFC-11 concentrations observed at remote measurement sites was constant from 2002 to 2012 and then slowed by about 50% after 2012. The observed slowdown in the rate of decline in atmospheric CFC-11 concentration was concurrent with a 50% increase in the mean concentration difference observed between the hemispheres and with the emergence of strong correlations at the Mauna Loa Observatory between concentrations of CFC-11 and other chemicals associated with anthropogenic emissions. A simple model analysis of our findings suggests a 13 ± 5 Gg/y (25 ± 13%) increase in CFC-11 emissions since 2012 despite reported production being near-zero since 2006 (4). Our three-dimensional model simulations confirm the increase in CFC-11 emissions, but indicate that it may have been as much as 50% smaller as a result of changes in stratospheric processes or dynamics. The increase in CFC-11 emission appears unrelated to past production, suggesting unreported new production, which is inconsistent with the Montreal Protocol agreement to phase out global CFC production.

Global production for dispersive uses of chlorofluorocarbons (CFCs), the class of chemicals contributing most to atmospheric chlorine, was fully phased out by 2010 (4). In the absence of production, steady declines in CFC emissions are expected as the reservoir of chemical remaining in existing equipment and products (CFC "banks") gradually escapes to the atmosphere and diminishes. Declines in atmospheric concentrations follow, after emission becomes smaller than atmospheric destruction. Expectations for stratospheric ozone concentrations returning to 1980 levels by mid-century rely on continued declines

in emissions and atmospheric concentrations (or mole fractions) of ozone-depleting gases, particularly CFCs.

For CFC-12 and CFC-113, two of the three most abundant CFCs, measured declines in atmospheric mole fractions over the past two decades have slowly approached lifetime-limited rates, consistent with diminishing production, emission, and banks. Hemispheric mole-fraction differences, which arise because emissions are predominantly from the northern hemisphere (NH), were also approaching zero[1].

For CFC-11, this conceptual framework explains atmospheric changes observed from 1995 to 2002 reasonably well, as production dropped below annual emissions and the bank of CFC-11 (1420 Gg in 2008, mostly in foams[5]) diminished, sustaining fewer emissions each year (Extended Data Table 1). After 2002, as reported production for all uses gradually decreased to zero, atmospheric rates of decline were projected to accelerate by a factor of 1.5 - 2 in response to the CFC-11 foam bank becoming depleted even more rapidly[6,7] (Figs 1, 2). Accelerated declines were not observed, however, as global CFC-11 mole fractions declined at a steady year-to-year rate of –2.1 ± 0.3 (1 s.d.) ppt/y (or –0.85 ± 0.10 %/y) in the decade following 2002 (1,8) (Fig. 1), suggesting a gap in our understanding of CFC-11 sources and sinks since the early 2000s.

The gap between expectations and observations widened substantially after 2012, when CFC-11 global mole fractions began decreasing even more slowly. In recent data, *i.e.* from mid-2015 to mid-2017, the mean rate of change for CFC-11 (–1.0 ± 0.2 ppt/y, or –0.4 ± 0.1 %/y) was about 50% slower than observed during 2002-2012; it also was much slower than has been recently projected[7] (Fig. 1). This slowdown was observed by all three measurement systems at NOAA, and it was accompanied by a 50% increase in the mean hemispheric mole-fraction difference measured for CFC-11 (Fig. 1, Extended Data Fig. 1). The last time hemispheric differences and global rates of change of these magnitudes were observed for CFC-11 was nearly two decades ago (Figs 1b, 1c). Other long-lived gases do not show changes in global rates or interhemispheric differences that are as large or sustained as those observed for CFC-11 (Extended Data Fig. 2).

For long-lived chemicals emitted primarily in the NH, concentration differences between hemispheres are highly correlated with global emission rates, although these differences are also influenced by rates of air exchange between the northern and southern hemispheres (SH) and any hemispheric asymmetry in stratosphere-troposphere exchange[9] (STE). Our analysis of other anthropogenically-produced and emitted gases suggests no appreciable weakening in tropospheric NH-SH exchange in recent years

(Extended Data Fig. 3), indicating that the recent changes observed uniquely for CFC-11 most likely arise from a sustained increase in the net flux of CFC-11 to the NH troposphere.

The slower global decline in CFC-11 mole fractions after 2012 represents a ~20% perturbation in the balance of CFC-11 sources and sinks. Considered together, the observational evidence implies either an increase in NH CFC-11 emission, a decrease in stratospheric loss rates or reduced STE primarily in the NH, or some combination of these effects. When analyzed with a three- or twelve-box model and constant tropospheric and STE dynamics, measured global atmospheric changes imply a steady decrease in emissions in the 15 years before 2002 from a late-1980s peak of ~350 Gg/y, relatively constant emissions from 2002 to 2012 at 54 ± 3 Gg/y, and a mean emission rate during 2014-2016 of 67 ± 3 Gg/y, which is 13 ± 5 Gg/y or 25 ± 13 % above the 2002-2012 mean (Fig. 2; see Methods). The post-2012 hemispheric differences and emission magnitudes are similar to those derived for the late 1990s and are well represented by the 3-box model (Extended Data Fig. 4). These results indicate consistency in two separate features of the measurements (trend and distribution) for all recent years and support the conclusion that NH emissions of CFC-11 have increased, although they do not rule out some contribution from changing stratospheric processes or STE dynamics.

Additional evidence for increasing NH CFC-11 emissions after 2012 comes from the emergence at the Mauna Loa, Hawaii Observatory (MLO) of enhanced variability in CFC-11 mole fractions and strong correlations between mole fractions of CFC-11 and other chemicals with anthropogenic emissions (Fig. 3; Extended Data Figs 5-7). Tropospheric ozone trends measured at MLO have revealed a significant influence of Eurasian emissions in autumn when stratospheric influences are relatively small[10]. We find strong correlations at MLO during autumn in mole fractions of anthropogenically-produced gases emitted in substantial quantities, particularly from East Asia[1] (*e.g.*, HCFC-22, and CH_2Cl_2), with slopes roughly consistent with relative emission rates derived elsewhere[11]. Back trajectory analyses confirm that MLO sampling events exhibiting enhanced mole fractions of these chemicals are associated with increased sensitivity to surface emissions from East Asia. But while similarly high correlations are observed at MLO during autumn among these pollution-related chemicals including carbon monoxide in all years since 2009, high correlations are observed for CFC-11 and these pollution tracers only after 2012.

While this evidence strongly argues for increased CFC-11 emissions from East Asia after 2012, changes in the CFC-11 lifetime or STE dynamics could influence the magnitude of emissions derived with the simple model approach. Given that the strength of stratospheric circulation can vary (*e.g.*, following the year

2000; 12, 13), and recent documented changes in stratospheric transport and STE[14-17] including the presence of a substantial El Niño in late 2015 to early 2016 (18), we simulated CFC-11 mole fraction changes in two 3-dimensional chemistry-climate models (CCMs) with three representations of reanalyzed meteorology from 2000 through 2016 and, in some simulations, 2017 (19-21) (Methods).

When forward CCM simulations include the CFC-11 emission history derived from the 3-box model, the rate of change simulated in the CCM for global CFC-11 mole fraction is consistent with observations from 2000 to 2012. After 2012, however, a discrepancy becomes apparent, with simulated mole fractions declining more slowly (Fig. 4a, Extended Data Fig. 8). This discrepancy becomes much smaller when dynamics in 2012 are repeated in subsequent years, suggesting that changes in transport contributed to the slower decline observed for CFC-11 during 2014-2016; transport anomalies had much less influence on the simulated rate of change in 2017. Transport anomalies cannot entirely explain the slower decline observed after 2012, however, because simulated CFC-11 mole fractions decline too quickly in CCM runs with emissions kept constant after 2012.

Known uncertainties in CCMs and reanalysis meteorology[22] and model-dependent differences in our simulation results (Extended Data Fig. 8) preclude a robust estimate of dynamical influences on derived emissions. The comparison of observed rates of change to those simulated with constant and increasing emissions (Fig. 4a) suggests that the emission increase derived for 2014-2016 in the 3-box model may be overestimated by as much as 50%.

We also considered CCM simulations of CFC-113 and CFC-12 (Extended Data Fig. 2). The CCM simulations showed no persistent bias throughout 2014 to 2016, suggesting that the mismatch observed for CFC-11 is unique.

Further evidence for increased CFC-11 emissions is supplied by considering changes in the hemispheric mole fraction difference after 2012. Simulated hemispheric differences increase analogously to observations only in response to increasing emissions (Fig. 4b, Extended Data Fig. 8). When emissions are kept constant after 2012 the simulated N–S mole fraction difference does not increase, implying that changes in dynamics cannot explain the increase in the N-S difference observed then. The magnitude of the post-2012 increase in interhemispheric difference in CCM simulations we considered was both smaller and larger than was measured. Simulations yielding larger differences in N–S mole fraction than observed would be more consistent with the post-2012 emissions increase being overestimated by the 3-box analysis, but are only derived with emission distributions considered less

likely in recent years (Methods). This apparent discrepancy may stem from simulated hemispheric mole fraction differences being more sensitive to uncertain model details (*e.g.*, emission distribution) and simulated processes (*e.g.*, interhemispheric mixing timescales and STE) than are rates of change in surface mole fractions (Fig. 4; Extended Data Fig. 8c,8f,8i).

It seems unlikely that the increased CFC-11 emissions are related to faster releases from banks or from inadvertent production. Increases in bank-related emissions are thought possible from demolition of buildings containing CFC products, although these emissions are expected to be small and only slowly increase over time[23]. Furthermore, increasing CFC emissions from building decommissioning is anticipated initially in developed countries where most CFC-11 was used in the 1970s, yet atmospheric measurements suggest, for example, a decline in U.S. emissions from 2008 to 2014, consistent with inventories[24] (a qualitative update suggests no significant emission increases after 2014). If reported production values are accurate, our results would require a doubling in the fractional release rate from CFC banks over the past 15 years and a significant increase in emissions from banks over only a few years' time, both of which seem improbable (Fig. 2b; Extended Data Fig. 9).

Inadvertent CFC-11 production is also possible from the fluorination of chlorinated methanes (*e.g.*, to produce HCFC-22), although we would expect this amount to be fairly small and that most, if not all, of CFC-11 produced in this manner would be captured and recycled or destroyed.

These considerations suggest that the increased CFC-11 emissions arise from new production not reported to UNEP's Ozone Secretariat, which is inconsistent with the agreed phase out of CFC production in the Montreal Protocol. Increased CFC-11 emissions augment the long-lived chlorine (Cl) burden of the atmosphere and stratospheric ozone depletion rates. The recent emission increase has slowed the decline in total tropospheric Cl by ~3 ppt/y (~22% considering 2008 to 2013 mean rate[1]) over the past three years. Other threats to stratospheric ozone identified recently are substantially smaller[25] or relate to influences that could be reversed on short time scales[11,26]. This is the first time emissions of one of the three most abundant, long-lived CFCs have increased for a sustained period since production controls took effect in the late 1980s. A delay in ozone recovery and an increase in climate forcing is anticipated, with an overall significance depending on the trajectory of CFC-11 emissions and concentrations in the future.

1. Carpenter, L.J. *et al*. in *Scientific Assessment of Ozone Depletion 2014, Global Ozone Research and Monitoring Project - Report No. 55.* Chapter 1, 1.1–1.101 (World Meteorological Organization, Geneva, Switzerland, 2014).

2. Montzka, S.A. *et al*. Decline in the tropospheric abundance of halogen from halocarbons: Implications for stratospheric ozone depletion. *Science* **272**, 1318-1322 (1996).

3. Prinn, R.G. *et al*. A history of chemically and radiatively important gases in air deduced from ALE/GAGE/AGAGE. *J. Geophys. Res*. **105**, 17751-17792 (2000).

4. http://ozone.unep.org/Publications/MP_Handbook/MP-Handbook-2012.pdf

5. Technology and Economic Assessment Panel, Task Force Decision XX/8 Report, Assessment of Alternatives to HCFCs and HFCs and Update of the TEAP 2005 Supplement Report Data, coordinated by L. Kuijpers, and D. Verdonik, United Nations Environment Programme, Nairobi, Kenya, available: http://ozone.unep.org/teap/Reports/TEAP_Reports/teap-may-2009-decisionXX-8-task-forcereport.

6. Daniel, J. *et al*., in *Scientific Assessment of Ozone Depletion 2010, Global Ozone Research and Monitoring Project - Report No. 52.* Chapter 5, 5.1–5.56 (World Meteorological Organization, Geneva, Switzerland, 2011).

7. Harris, N. R. P. *et al*. in *Scientific Assessment of Ozone Depletion 2014, Global Ozone Research and Monitoring Project - Report No. 55.* Chapter 5, 5.1–5.58 (World Meteorological Organization, Geneva, Switzerland, 2014).

8. Montzka, S.A. *et al*., in *Scientific Assessment of Ozone Depletion 2010, Global Ozone Research and Monitoring Project - Report No. 52.* Chapter 1, 1.1–1.108 (World Meteorological Organization, Geneva, Switzerland, 2011).

9. Liang, Q. *et al*. Constraining the carbon tetrachloride (CCl_4) budget using its global trend and inter-hemispheric gradient. *Geophys. Res. Lett.* **41**, 5307-5315 (2014) 10.1002/2014GL060754.

10. Lin M., Horowitz, L.W., Oltmans, S.J., Fiore, A.M., Fan, S. Tropospheric ozone trends at Mauna Loa Observatory tied to decadal climate variability. *Nature Geosci*. 7, 136-143 (2014) 10.1038/NGEO2066.

11. Oram, D.E *et al.* A growing threat to the ozone layer from short-lived anthropogenic chlorocarbons. *Atmos. Chem. Phys*. **17**, 11929-11941 (2017) 10.5194/acp-17-11929-2017.

12. Rosenlof, K. R. & Reid, G.C. Trends in the temperature and water vapor content of the tropical lower stratosphere: Sea surface connection. *J. Geophys. Res*. **113**, D06107 (2008) 10.1029/2007JD009109.

13. Randel, W. J., Wu, F., Vömel, H., Nedoluha, G.E., Forster, P. Decreases in stratospheric water vapor after 2001: Links to changes in the tropical tropopause and the Brewer-Dobson circulation. *J. Geophys. Res*. **111**, D12312 (2006) 10.1029/2005JD006744.

14. Ploeger, F. *et al*. Variability of stratospheric mean age of air and of the local effects of residual circulation and eddy mixing. *J. Geophys Res.* **120**, 716-733 (2015) 10.1002/2014JD022468.

15. Stiller, G.P. *et al.* Shift of subtropical transport barriers explains observed hemispheric asymmetry of decadal trends of age of air. *Atmos. Chem. Phys. Discuss*., in press (2017) 10.5194/acp-2016-1162.

16. Newman, P.A., Coy, L., Pawson, S. & Lait, L.R. The anomalous change in the QBO in 2015-2016. *Geophys. Res. Lett*. **43**, 8791-9797 (2016) 10.1002/2016GL070373.

17. Chirkov, M. *et al*. Global HCFC-22 measurements with MIPAS: retrieval, validation, global distribution and its evolution over 2005-2012. *Atmos. Chem. Phys.* **16**, 3345–3368 (2016) 10.5194/acp-16-3345-2016.

18. https://www.esrl.noaa.gov/psd/enso/mei/

19. Marsh, D.R. *et al*. Climate change from 1850 to 2005 simulated in CESM1(WACCM). *J. Clim.* **26**, 7372-7391 (2013) 10.1175/JCLI-D-12-00558.1.

20. Lamarque, J.-F. *et al*. CAM-chem: description and evaluation of interactive atmospheric chemistry in the Community Earth System Model. *Geosci. Model Dev*. **5**, 369-411 (2012) 10.5194/gmd-5-369-2012.

21. Rienecker, M.M. *et al*. MERRA: NASA's modern-era retrospective analysis for research and applications. *J. Clim*. **24**, 3624-3648 (2011) 10.1175/JCLI-D-11-00015.1.

22. Boothe, A.C. & Homeyer, C.R. Global large-scale stratosphere-troposphere exchange in modern reanalyses. *Atmos. Chem. Phys.* **17**, 5537-5559 (2017) doi:10.5194/acp-17-5537-2017.

23. Ashford, P. *et al.* Foams. Chapter 7 in IPCC/TEAP Special Report on Safeguarding the ozone layer and the global climate system, issues related to hydrofluorocarbons and perfluorocarbons, Cambridge Univ. Press, NY (2005).

24. Hu, L. *et al*. Considerable contribution of the Montreal Protocol to declining greenhouse gas emissions from the United States. *Geophys. Res. Lett*. **44**, (2017) 10.1002/2017GL074388.

25. Laube, J.C. *et al*. Newly detected ozone-depleting substances in the atmosphere. *Nature Geosci.* **7**, 266-269 (2014) 10.1038/ngeo2109.

26. Hossaini, R. *et al.* The increasing threat to stratospheric ozone from dichloromethane. *Nature Comms*. **8** (2017) 10.1038/ncomms15962.

Acknowledgements For sample flask collection and on-site instrument operation, maintenance, and troubleshooting we are grateful to NOAA station personnel. We also are indebted to personnel from cooperative institutions involved with flasks sampling in Australia (CSIRO), Canada (AES), Ireland (U Bristol), Israel (Weizmann Inst.), U.S. (Univ. of Colorado, Harvard University, University of Wisconsin, Scripps Institute for Oceanography), and for logistics support from the U.S. National Science Foundation (NSF) at Summit, Greenland and South Pole. We appreciate useful discussions with J. Butler, D. Fahey, S. Reimann, P. Newman, and AGAGE scientists; S. Davis for MERRA2 reanalysis winds; and P. Novelli for CO data from MLO. The CESM project is supported by the NSF and the Office of Science (BER) of the U.S. Department of Energy. The authors acknowledge the NOAA Research and Development High Performance Computing Program for computing and storage resources. This work was funded in part by the NOAA Climate Program Office's AC4 program.

Author contributions S.A.M. led the investigation, provided GCMS measurements, performed interpretive analysis and box modeling; G.S.D., D.J.N., and D.M. provided GCECD measurements; C.S. and B.R.M. provided GCMS measurements; D.J.N. and M.R. performed 12-box modeling; P.Y., R.W.P. performed CCM simulations; J.S.D., E.R., and F.M. performed box modeling and provided conceptual understanding; B.D.H. ensured accuracy and consistency in standard scales; L.K. provided insight into UNEP reporting; L.H. provided data analysis; A.J.M. performed trajectory calculations; S.A.M. wrote the paper with input from J.S.D., M.R., P.Y., L.K., B.D.H., G.S.D., J.W.E., and L.H.

Author information The authors declare no competing financial interests.

1 National Oceanic and Atmospheric Administration, Boulder, Colorado 80304, USA.

2 Cooperative Institute for Research in Environmental Sciences, University of Colorado, Boulder, Colorado, 80309, USA.

3 Technical University Eindhoven, Eindhoven, 5612 AZ, The Netherlands.

4 School of Chemistry, University of Bristol, Bristol, BS8 1TS, UK

5 United Kingdom Met Office, Exeter, EX1 3PB, UK.

Figure 1| Observations of atmospheric CFC-11 over time. **a**, Hemispheric mean mole fractions estimated for the northern (red lines) and southern hemisphere (blue lines); different shades of red or blue represent results from a total of three different instruments (see Methods). **b**, Inferred rate of change on the measured global CFC-11 mole fraction. **c**, Measured differences in hemispheric mean mole fraction. In **b** and **c**, line colors represent results from flask GCMS (brown), flask GCECD (green) and, in **b** only, in-situ GCECDs (thick grey). In **a** and **b**, grey numbered thin lines represent projections from recent WMO Assessment scenarios (as global means) given the data available at the time the scenarios were created [6,7,27].

Figure 2| Global CFC-11 emission, reported production, and implied release rate from CFC-11 banks. **a**, Production magnitudes reported to UNEP[4] (green line) are compared to emissions derived from atmospheric data with a 3-box (black squares) or 12-box model (blue line) considering a 57.5 y lifetime (Extended Data Table 1). Also shown is an independent emission history constrained by NOAA and AGAGE observations through 2012 and is the WMO scenario projection thereafter[1,7] (grey solid line; rescaled for a 57.5 y lifetime). Uncertainties on 3-box emissions represent 1 s.d. of the sum of squares of a bootstrap analysis plus the spread in estimates from multiple instruments (see Methods). **b**, The implied annual release fraction of CFC-11 from its banks, considering i) the UNEP production and 3-box-derived emission histories in **a** (black squares; see Methods); ii) same as (i), but with the atmosphere-derived emission increase after 2012 reduced by 50% to represent potential dynamical contributions to that increase (blue dashed line in **a** and **b**); iii) a constant release fraction from the bank of 3.2% after 2002 (grey dashed lines); and iv) constant emissions at 54 Gg/y from 2002 to 2016 (red line). See also Extended Data Fig. 9.

Figure 3| Covariations in mole fractions of CFC-11 and HCFC-22 measured at MLO and air transport differences influencing this variability. **a** Mole fractions of CFC-11 and HCFC-22 measured by GCMS in weekly flask pairs in 2010 at MLO; uncertainties represent 1 s.d. of flask pair means. **b**, Same as **a**, but for 2016. **c**, The annual regression coefficients (r^2) associated with results from MLO during autumn (fraction of year >0.6 and <0.9): CFC-11 *vs*. HCFC-22 (squares), CFC-11 *vs*. CH_2Cl_2 (crosses), and HCFC-22 *vs*. CH_2Cl_2 (plusses). **d** & **e**, A back-trajectory analysis[28] showing surface regions sensed by the 2016 sampling events at MLO labeled L1 and H1 in **b**, with darker colors indicating greater influence. Color scale is logarithmic and represents the calculated time-averaged concentration within the surface layer (0 – 2000 m) during the 30 days prior to the sampling events given a point release at MLO of 1 g/s. See also Extended Data Figs 5-7.

Figure 4| CFC-11 rates of change and hemispheric differences. **a**, CFC-11 global rates of change derived from observed (red symbols and lines; shaded region indicates 1 s.d. of 3-y running mean in observations) or simulated mole fractions (blue, green, black lines). Simulations were performed with the CAM CCM, MERRA2 reanalysis meteorology, and emission histories either from 1) the 3-box model (blue lines labeled "E1"), or 2) E1 emissions kept constant at the 2012 rate after 2012 (green lines labeled CE). Simulation with the latest WMO emission projection[1] based on observations through 2012 using WACCM and MERRA1 appear as the black line. Simulations were also performed with 2012 dynamics applied to years after 2012 (dashed blue and green lines labeled FD for "fixed dynamics"). **b**, the change since 2010 in observed and simulated interhemispheric mole fraction difference relative to the 2010-2012 mean (note expanded x-axis scale). Colors in common with panel **a** refer to results obtained with those same methodologies, although only flask results are considered in **b**. CCM-simulation results are labeled as x/y/z, where x refers to how global emissions derived from the 3-box model were distributed spatially (E1=Emission1, *etc*., see Methods), y refers to the reanalysis meteorology (M2=MERRA2, M1=MERRA1) and z refers to the model used. Additional dotted grey lines in **b** represent results from simulations with CAM and MERRA2 in which the entire post-2012 emission increase derived in the 3-box model was distributed evenly throughout Europe (EU), the United States (US) or Asia (Asia) (see Methods and Extended Data Fig. 8). Observations are from flasks analyzed by GCECD (red line, unfilled diamonds), GCMS (red line, filled circles) and, in **a** only, in-situ instrumentation (red lines).

Methods.

Observations. We have measured CFCs and other trace gases in ambient air at multiple sites throughout the globe for over two decades by three different methods[1,2] (Extended Data Table 1). At two remote sites in the southern hemisphere (SH) and four remote sites in the northern hemisphere (NH), air is collected and analyzed multiple times per day by automated onsite instrumentation with gas chromatography coupled with electron capture detection (GCECD). At those and other remote sites (12 total) paired glass or stainless-steel flasks are collected approximately weekly when winds are from a clean air sector. These flasks are analyzed in our Boulder laboratories on two separate gas chromatography instruments using different columns and detectors: separation on a 10% SP-2100 packed column followed by ECD, and separation on a 60m 0.25 mm ID with a 1μ DB-5 film thickness capillary column followed by mass spectrometry detection (GCMS) primarily on ion $C^{35}Cl^{37}ClF^{+}$ (m/z = 103). Flask air has also been analyzed on additional GCMS instruments using a 0.32 mm ID GasPro column. Results from these instruments show similar distributions, rates of change, and trace-gas correlations so are not discussed further.

Consistency over time in the GCMS standard scale is maintained independently from GCECD instruments. For GCMS data, the scale is maintained by the sequential analysis of a suite of high-pressure real-air samples in treated aluminum cylinders. Consistency in that scale is assessed by repeat analysis of real humidified air in a separate suite of eight high-pressure, electropolished stainless steel cylinders, and is estimated to be better than 0.1 ppt over 2010-2017. A measure of the consistency in results from GCECD instrumentation (field instruments and the flask analysis instrument) is provided by repeat analyses of gravimetrically-prepared standards and an independent suite of high-pressure real-air samples on a common laboratory-based ECD instrument in Boulder; it is estimated to be 0.2 ppt (1-s.d.) over the 2010 to 2017 period.

Results from all three measurement systems are tied to a suite of standards prepared in house with gravimetric techniques spanning 100 to 260 ppt CFC-11 (29). These standards enable the accurate characterization of instrument response over the range of measured ambient CFC-11 mole fractions. Comparisons with other global observations[1] indicated NOAA ECD results for CFC-11 declining ~0.2ppt/y faster than those from one international sampling program from 2008 to 2012 (the Advanced Global Atmospheric Gases Experiment[3]), although this divergence has become insignificant with the NOAA ECD CFC-11 scale revision in 2016.

GCMS measurements from flasks significantly improved after a detector upgrade in 2009 (median flask pair agreement was 0.4 ppt before 2009 and has been 0.25 ppt or 0.1% afterwards). GCMS results from mid-2008 to mid-2009 suffer from detector problems so we focus here on post-2009 data from this instrument.

Data treatment. Monthly mean mole fractions are derived from flask pairs sampled during the month; the small fraction (typically < 5%) of results deemed unrepresentative of the background atmosphere based on variability in sequential measurements and results from nearby sites are not considered additionally. Hemispheric means are derived by weighting results by cosine of sampling latitude, except for South Pole, for which a weight of 0.4 is used to give South Pole results an equivalent weight to those from Palmer Station. In our experience results from these sites are similarly representative of CFC mole fractions in the high-latitude SH.

The global rate of change quoted for CFC-11 mole fractions during 2002-2012 is the mean and 1 s.d. of the 10 year-to-year differences measured for the global mean surface mole fraction (relative rates determined as $\ln(\text{mean}_{y2}/\text{mean}_{y1})$). In all figures, rates and hemispheric mole fraction differences are displayed as running 12-month means and are plotted at the end of the 12-month intervals. We consider hemispheric differences estimated only from flask measurements because small inter-site differences are more reliably determined when samples from different sites are analyzed with a single instrument and because the estimates are more accurate when derived from the larger number of flask collection sites.

3-box model for deriving emissions. Calculations were performed with a 3-box model with boxes representing the northern and southern hemisphere troposphere, separated at the equator, and the stratosphere. The model includes a timescale for exchange between tropospheric boxes of 1.1 y, a timescale for mass exchange between the stratosphere and troposphere of 2 y (with 55% occurring in the NH and 45% in the SH), although our conclusions do not depend strongly on these particular values. Emissions were distributed so that 95% were in the northern hemisphere troposphere[20,31]. The loss rate constant in the stratospheric box was adjusted to provide a steady-state lifetime matching the mean CFC-11 lifetime diagnosed in the CCMs (56, 57.5, or 62 y depending on model). While these lifetimes are slightly longer than the best estimate (52(43-67) y (1)), they are well within this range. Emissions derived with this model are indistinguishable from those derived with other models when similar observations and lifetimes are considered[1,32] (Fig. 2).

Uncertainties on measurement-based estimates of global annual mean mole fractions affect our ability to assess changes in emissions over time. In GCMS flask results, site-specific standard deviations on monthly means ranged between 0.08 to 0.14% (1 s.d.) at the 12 remote sites used in this study when averaged over 2010-2017; the variability in sequential monthly means at these sites is another measure of uncertainty and is even smaller (0.02 to 0.04%, 1 s.d.). Uncertainties on global annual means were estimated with a bootstrap technique using replacement. This involved estimating global annual mean mole fractions from a random selection of sites in the network, and uncertainties on monthly site means were also included. The only requirement of each randomly selected network was that it include >1 SH site. Uncertainties (1 s.d.) on these global means ranged from 0.1 to 0.2 ppt (0.05 to 0.1%), which corresponds to an annual emission uncertainty (1 s.d.) ranging from 1.5 to 3 Gg/y.

The difference between average emissions derived during 2002-2012 and 2014-2016 was estimated to be 13 ± 5 Gg. The uncertainty on this value includes ±1.5 Gg for a CFC-11 lifetime range of 43-67 y (1). Additional error included in the ±5 Gg uncertainty was estimated with three different approaches that yielded consistent values: from the sum of squares of emission variability in mean emissions derived for these two periods with the 3-box model from the three instrumental methods; from those derived from a bootstrap analysis of global annual mean uncertainties (discussed above); and from those derived from the 12-box model (see below).

The relative uncertainty on the emission increase (*i.e.*, when stated relative to the mean 2002-2012 emission) includes a lifetime dependence on the pre-2013 emissions assuming a lifetime of 57.5 y and an error associated with loss derived for the lifetime range quoted above. When derived with a 52 y lifetime, the mean emission during 2014-2016 is estimated to be 21 ± 11% higher than mean emissions during 2002-2012.

Uncertainty related to the accuracy of the surface network to represent full tropospheric mean mole fractions and their change over time was assessed with CCMs. The bias is a function of emission magnitude and, when averaged over 2014-2016, was approximately +1 Gg/y, or well within the uncertainties listed in Table 1 and those on the derived emission increase. Consideration of CCM results also suggests that mean hemispheric differences estimated from our sampling network overestimate the tropospheric column hemispheric difference in all years by 0.5 to 0.75 ppt. This bias is substantially reduced (0.2 ppt) when N–S differences are considered relative to the 2010-2012 mean. As a result, all comparisons performed between measurement-based and CCM-simulated interhemispheric mole-

fraction differences (*e.g.*, Fig. 4 and Extended Data Fig. 8) were performed by extracting mole fractions from CCM-simulated mole fraction fields at site-specific locations and treating those results as we did observations to derive hemispheric and global means. Furthermore, considering changes in the N–S difference relative to the 2010-2012 mean minimizes errors associated with the spatial distribution of pre-2012 CFC-11 emissions on our analysis (*e.g.*, see Extended Data Fig. 8). Finally, changes in site-derived hemispheric differences were found to be very consistent with hemispheric differences when derived from simulated mole fractions in all near-surface model grid cells.

Emission histories were similarly derived for CFC-12 and CFC-113 using our observations, the 3-box model, and lifetimes matching those diagnosed in the CCMs. Those emission histories were also used as input in forward runs of the CCM simulations. These gases were considered in assessing the CCM simulations even though STE influences on tropospheric mole fractions are dependent on chemical lifetime.

Bank release rate calculation. The annual release fraction of CFC-11 from its banks was derived from the emission and production histories shown in Fig. 1 and a CFC-11 bank totaling 1420 Gg in 2008 (5). The absolute value of this rate is dependent on the CFC-11 lifetime. An analysis of emission histories derived for lifetimes within the most likely range (43-67 y) suggests a lifetime-independent conclusion: if the CFC-11 production history is accurate, the annual bank release rate would have had to approximately double during the past decade in the absence of unreported production (Extended Data Fig. 9). Considering the reporting to UNEP of quantities of CFC-11 that have been destroyed does not change this conclusion (Extended Data Fig. 9). Given the unlikely potential for this substantial increase, we conclude that the emission increase is more likely due to unreported production (see text).

12-box model for deriving emissions. Estimates of CFC-11 emissions were also made using a two-dimensional, 12-box model of atmospheric transport and chemistry and observations from ECD measurements or from GCMS data[32]. In each vertical level, the model consists of four equal-mass boxes separated at 30 degrees north and south and at the equator. Vertical divisions are at 500 hPa and 200 hPa. Stratospheric loss rates were tuned such that the annual-mean global lifetime was 56 y, consistent with 3D model predictions. Emissions were estimated for each season in each model semi-hemisphere between 1994 and 2016, using a least-squares fit to the data (*e.g.*, with no prior constraint on the emissions). Model transport parameters were tuned to produce similar semi-hemispheric background mole fractions to long-term means in a 3D model and were assumed to be inter-annually repeating[32].

Monthly, semi-hemispheric means were calculated from the data for comparison with the model. The uncertainty on each of these averages was assumed to be the quadratic sum of the measurement repeatability and the variance in the observed monthly averages across sites within each semi-hemisphere. The latter term represents an estimate of the model "mismatch" error, which was here assumed to be due to the lack of spatial resolution in the model. No systematic uncertainties were included in the emissions uncertainty estimate (*e.g.* uncertainties due to lifetime or calibration scales), because the primary focus of this work is to understand changes in inferred emissions, rather than their absolute magnitudes; uncertainties related to variations in transport and transport-derived changes in loss are considered in the CCM simulations (see below). The emission uncertainties calculated in this manner were similar to those calculated from the bootstrap analysis of the observations in the 3-box model analysis.

Chemistry-climate model simulations. CCM simulations were performed to assess the role of changing atmospheric processes (chemistry and dynamics) on CFC-11 mole fractions. Biases noted between observed mole fractions and those from CCM simulations potentially indicate changes in atmospheric dynamics; such influences also became apparent from simulations performed with repeating reanalysis meteorology.

CFC-11 mole fraction histories were calculated in forward simulations in the Whole Atmosphere Community Climate Model (WACCM)[19], and the Community Atmosphere Model (CAM) 5.3 (20) of the Community Earth System Model (CESM1), version 1. Models were run at 1.9° latitude x 2.5° longitude horizontal resolution with 88 vertical levels from Earth's surface to $6x10^{-6}$ hPa. Horizontal winds and temperatures are nudged to specified dynamics derived from three different reanalysis products including the Modern Era Retrospective-analysis for Research and Applications (MERRA[21]), MERRA2, and the Goddard Earth Observing System Data Assimilation System Version 5 (GEOS5). A separate run in which only the model winds were nudged (not temperature) was also performed with MERRA2 in CAM5 (UV-only nudge results in Extended Data Fig. 8).

Global mole fractions and distributions of CFC-11 and other CFCs were initialized in the year 2000. Three different emission histories were considered thereafter: 1) emissions estimated from the 3-box analysis of observations for all years given a steady-state lifetime matching that diagnosed from the particular CCM and meteorology, 2) same as in case #1, but with emissions kept constant during 2013-2016 at 2012 rates, and, for CFC-11 only, 3) emissions projected from the most recent WMO Ozone

441 Assessment[1] (rescaled to the lifetime considered here). Emission magnitudes used for 2017 simulations
442 were assumed unchanged from 2016 values, given that the observational data required to derive 2017
443 emissions are not yet available (data through mid-2018 are required with the existing methodology).

444 Multiple spatial distributions of CFC-11 emissions were also used in CCM simulations to test the
445 sensitivity of simulated hemispheric difference on those distributions. The distributions include a span
446 of 90 to 96.1% in the fraction of total emission from the NH (or 85 to 95% in the fraction of emission
447 north of 10°N), which encompasses previous estimates based on production data[28,29]. Total global
448 emissions were distributed in each year as follows: Emission1 = evenly distributed across land surfaces
449 in the zonal bands as follows: 0% from 90°N to 60°N, 5% from 60°N-50°N, 80% from 50°N-25°N, 12%
450 from 25°N-10°S, 3% from 10°S-40°S, 0% from 40°S-90°S (equivalent to 90% of emission north of 10°N);
451 Emission2 = 0% from 90°N to 60°N, 5% from 60°N-50°N, 80% from 40°N-10°N, 10% from 10°N-10°S, 5%
452 from 10°S-40°S, 0% from 40°S-90°S (equivalent to 85% of emission north of 10°N); and Emission3 = the
453 GEIA emission distribution[31] (equivalent to 95% of emission north of 10°N). The sensitivity of emission
454 location on our simulated results was also tested in three 'tagged-tracer' experiments in which the CFC-
455 11 emission magnitude above the 2010-2012 average was distributed evenly in years after 2012
456 throughout regions representing Asia (20°N-40°N, 90°E-120°E), the United States (20°N-50°N, 60°W-
457 120°W) or Europe (30°N-60°N, 0-60°E); emissions in other regions in these simulations were kept
458 constant after 2012 (Fig. 4).

459 While accurate spatial distributions of CFC-11 are not well defined, they are estimated based on
460 country-scale reporting of CFC production and consumption to UNEP[4]. Given the phase-out of CFC
461 production first in developed countries, the CFC-11 emission distribution has likely shifted to more
462 southerly latitudes over time[30,31] and, therefore, become more like distribution Emission1 (or the Asian
463 region in tagged tracer experiments) rather than that prescribed in Emission2 or Emission3.

464 While the post-2012 emission increase in the NH averaged 13 Gg during 2014-2016 in these tagged-
465 tracer simulations, the NH emission increase was somewhat less (by up to 2 Gg) in the simulations using
466 emission distributions 1, 2, and 3 because these runs did not consider a changing emission distribution.
467 Emissions of CFC-12 and CFC-113 were distributed as in Emission1. Rates of change simulated for CFC-
468 11 with the 3-box-model-derived emissions were insensitive to lifetime, but had some dependence on
469 the model and choice of meteorology and nudging methodology (Extended Data Fig. 8a, d, h).

Data availability. Data used in this study are available at ftp://ftp.cmdl.noaa.gov/hats/cfcs/cfc11/ or from the corresponding author on reasonable request.

27. Montzka, S.A. *et al*., in *Scientific Assessment of Ozone Depletion 2002, Global Ozone Research and Monitoring Project - Report No. 47.* Chapter 1, 1.1–1.83 (World Meteorological Organization, Geneva, Switzerland, 2003).

28. Jones A.R., Thomson D.J., Hort M. and Devenish B. The U.K. Met Office's next-generation atmospheric dispersion model, NAME III, in Borrego C. and Norman A.-L. (Eds) Air Pollution Modeling and its Application XVII (Proceedings of the 27th NATO/CCMS International Technical Meeting on Air Pollution Modelling and its Application), Springer, pp. 580-589, 2007.

29. Hall, B.D., Dutton, G.S., Elkins, J.W. The NOAA nitrous oxide standard scale for atmospheric observations. *J. Geophys. Res*. **112**, D09305 (2007) doi:10.1029/2006JD007954.

30. McCulloch, A., Ashford, P., Midgley, P.M. Historic emissions of fluorotrichloromethane (CFC-11) based on a market survey. *Atmos. Environ*. **35**, 4387-4397 (2001).

31. Liang, Q., Stolarski, R.S., Douglass, A.R., Newman, P.A., Nielsen, J.E. Evaluation of emissions and transport of CFCs using surface observations and their seasonal cycles and the GEOS CCM simulation with emissions-based forcing. *J. Geophys. Res*. **113**, D14302 (2008) doi:10.1029/2007JD009617.

32. Rigby, M. *et al*. Re-evaluation of the lifetimes of the major CFCs and CH_3CCl_3 using atmospheric trends. *Atmos. Chem. Phys*. **13**, 2691-2702 (2013) 10.5194/acp-13-2691-2013.

Extended Data Table 1: Derived global emissions and global production of CFC-11.

Extended Data Figure 1| Hemispheric differences in CFC-11 mole fractions represented by results from individual sites at comparable latitudes. **a** 12-month running means of monthly differences are plotted at the mid-point of that time interval. Results from low latitudes (green lines) include a high altitude (MLO) and low altitude (KUM) site in the NH compared to SMO. Results from mid- to high-latitude site pairs are indicated in other colors and include data from high altitude (NWR, SUM, SPO) and low altitude sites (THD, MHD, BRW). Comparisons made at sites with similar sampling altitudes are indicated in bold lines. **b** Details of site locations where measurements of CFC-11 are obtained from flasks and from in-situ instrumentation.

Extended Data Figure 2| Observed and simulated global rates of change and hemispheric differences for some other long-lived chemicals. **a**, Measured global surface rates for N_2O (grey line), CFC-12 (blue thin lines), and CFC-113 (green thin lines) from flasks analyzed by GCECD and also, for the CFCs, the GCMS. **b**, Hemispheric differences measured for CFC-12 and N_2O, and in **c**, for CFC-113. Multiple CCM simulation results appear in **a**, **b**, and **c** for CFCs as thick dark lines and are updated only annually; they represent simulations using the CAMCHEM model with MERRA2 reanalysis meteorology and the 3-box-derived emission history. Dashed lines after 2012 represent simulations with emissions kept constant after 2012 (dark blue for CFC-12 or dark green for CFC-113), or when the 3-box-derived emission record was considered but dynamics in 2012 were repeated in subsequent years (red dashed lines). Emission distribution #1 was used in all simulations (see Methods).

Interannual variability in global growth rates for these gases are sometimes correlated, suggesting a common cause related to Stratosphere-Troposphere Exchange dynamics, perhaps associated with the quasi-biannual oscillation (QBO), although emission variations are particularly likely for N_2O (*e.g.*, 33-35). This may explain the peak in growth rates for a number of gases in 2015. The change in rate for CFC-11 (see Fig. 4), however, is substantially larger and is sustained in 2016 when rates for other gases do not change appreciably or become smaller, suggesting that the underlying causes for the majority of changes observed for CFC-11 are unique to that gas.

Extended Data Figure 3| The sensitivity of hemispheric mole fraction differences to variations in hemispheric air mass exchange. Points represent the observation-based (blue symbols) or modeled (red and grey symbols) hemispheric difference as a function of the global emission rate derived for that year in the 3-box model for HCFC-22 in **a**, and in **b**, for HFC-134a (see Methods; lines connect sequential years and the legend applies to **a** and **b**). The sensitivity of the N–S difference to exchange timescale ($\tau_{exch,\ N–S}$) was tested in the model by incorporating values of ± 0.1 y around 1.1 y. If this timescale did not vary inter annually, we would expect the observation-based points (blue) to overlay those from the model (red). A change in the annual mean value of this exchange would increase the difference between the observed and modeled N–S difference. Specifically, a ±0.1 year annual mean change would be reflected in the observed N–S difference being 2/3rds of the way closer to the grey point associated with the emission derived for that year. The consistency between the model (red) and observed (blue) hemispheric differences in most years suggests that inter-annual changes in the exchange timescale are 0.1 y (~10%) or less, typically. More importantly, the results show no systematic change in this relationship before and after 2012, suggesting that any change in the rate of hemispheric air exchange in the troposphere is <10% during this period. We estimate that to fit the observed increase in the N–S difference measured for CFC-11 after 2012 without increasing the net CFC-11 flux to the northern hemisphere, this exchange time constant would have had to increase from 1.1 to 1.7 y, which is inconsistent with the results presented here.

While the distribution of emissions between and within the hemispheres can affect the N–S difference, any significant change in this distribution over time would likely be to a shift to lower latitudes (away from the U.S. and E.U.) and would lead to a decrease in the N–S difference over time, not an increase

like what is observed for CFC-11 after 2012. Consistent with this, the best fit to the observations was obtained when the emission distribution (North / Globe) in these analyses was linearly decreased over time (from 0.95 in 1995 to 0.85 in 2015 for HFC-134a, and from 0.86 to 0.82 for HCFC-22). Assuming a constant hemispheric emission distribution (N/Globe) over time does not change the conclusions from this analysis.

Extended Data Figure 4| Measured and modeled annual hemispheric differences *vs.* global emissions of CFC-11. **a**, Measured N–S mole fraction difference as a function of the global emission derived with a 3-box model for 1978-2016; the line is a fit to all results and each point represents an annual mean for a particular year. **b**, An expanded scale of data displayed in **a** with results from different measurement methods represented by symbols of the same color; grey symbols (pluses and diamonds) refer to a combined set of results from flasks and *in situ* instruments analyzed by GCECD. For each method (color), unfilled symbols refer to results for the years 2010 to 2012; filled symbols refer to 2013-2016. Specific years are labeled for GCMS results during 2013-2016 and for ECD results during 1997-2000 (*e.g.*," '15" = 2015). The data show that the relationship observed here during 2014 to 2016 is similar to that observed during 1996-2000. **c**, Same as **b**, but with N–S differences derived from the 3-box model shown (black points and line connecting sequential years); select model years are labeled.

Extended Data Figure 5| Correlations between trace gases measured during autumn at Mauna Loa. **a,** Measured mole fractions of CFC-11 and HCFC-22 in all samples collected during autumn (fraction of year 0.6 – 0.9) at MLO in the past 9 years. **b**, Results for CH_2Cl_2 *vs.* HCFC-22 in those same samples and years. **c**, The r^2 regression coefficients (blue filled symbols, left-hand scale) and slopes (red unfilled symbols, right-hand scale) determined from the data in **a** over time. Only slopes for correlations that are significant at $p<0.05$ are shown (*i.e.*, those where $r^2 > \sim 0.25$). **d**, the same as **c**, but for data in **b** (CH_2Cl_2 *vs.* HCFC-22).

East Asia has been a substantial source of HCFC-22 and CH_2Cl_2 for a number of years[1,11]. As a result, significant correlated variability is expected in their mixing ratios downwind of this region; this is borne out in observations at MLO during autumn from 2009 to 2017. These data may also provide rough estimates of relative emission magnitudes. For example, inventory and atmosphere-based studies suggest emissions of HCFC-22 from China of ~100 Gg in 2010 increasing to 150 Gg in 2015 (1). Considering the slopes measured at MLO between HCFC-22 and CH_2Cl_2, this would correspond to regional emissions for CH_2Cl_2 of 300 Gg in 2010 increasing to 440 Gg in 2016. This is comparable to the 455 Gg (± 10%) estimated to have been used in China for emissive applications in 2015 (11). Applying the same analysis to CFC-11 suggest total emissions of 30-40 Gg/y in 2014-2017, or 10 to 35 Gg higher than estimated for Chinese CFC-11 emissions in 2008-2009 (considering errors; 1), which is of the same order as the global CFC-11 emission increase derived here for 2014-2016 (13 ± 5 Gg/y).

Extended Data Figure 6| Correlations between additional trace gases measured during autumn at Mauna Loa. Same as Extended Data Fig. 5, but for mole fractions of carbon monoxide *vs.* HCFC-22 measured at MLO during autumn. **a**, the results in individual years. **b**, The r^2 regression coefficients (blue filled symbols, left-hand axis) and slopes (red unfilled symbols, right-hand axis) determined from the data in **a** over the past 8 years.

Extended Data Figure 7| Variability in trace gas mole fractions measured at MLO before and after 2012. a Mole fractions of HCFC-22 measured in flasks collected at MLO during the autumn of 2011 (red lines and symbols) and 2016 (blue lines and symbols). **b**, The same as **a**, but for CFC-11. **c**-**f**, Back trajectories calculated[28] for 2011 samples indicated by the red text "L1", "L2", "H1", and "H2" in **a** and **b**.

g-j, Back trajectories calculated for 2016 samples indicated by the blue text "L1", "L2", "H1", and "H2" in **a** and **b**. In **c-j** darker shading represents surface regions sensed by the corresponding sampling events at MLO, with darker colors indicating greater influence. The color scale in the trajectory maps is logarithmic ($1x10^{-9}$ to $1x10^{-3}$ g-s/m^3, darker colors for higher concentrations) and represents the calculated time-averaged concentration within the 0-2000 m surface layer during the 30 days prior to the sampling event given a point release at MLO of 1 g/s (28). Elevated mole fractions of HCFC-22 are observed in both 2011 and 2016 (labeled H1 and H2 in **a** or **b** and High 1 and High 2 in **c-j**) when surface sensitivity over East Asia is enhanced; CFC-11 mole fractions at MLO co-vary with HCFC-22 in these East-Asian influenced samples only after 2012. Some industrialized regions (*e.g.*, Japan) have significant influence on samples containing both high and low mole fractions of CFC-11, HCFC-22, and CH_2Cl_2 and, therefore, are less likely the source of the enhanced CFC-11 mole fractions at MLO after 2012. These results, along with results from Fig. 3 and Extended Data Figs 5 & 6, suggest an increase in CFC-11 emissions from East Asia that is coincident with the increase in global emissions derived from our sampling network.

Extended Data Figure 8| Additional model simulations of CFC-11 mole fraction changes over time and of hemispheric differences. Rates of change and hemispheric differences from different combinations of emission distributions (E1, E2, E3), reanalysis meteorology [MERRA1 (M1), MERRA2 (M2), and GEOS5 (G5)], and CCMs (CAM and WACCM) are compared to quantities derived from observations (red lines or shading indicates the range of results from two (hemispheric differences) or three (global change rates) measurement techniques (Methods). In all panels, results from observations and the CAM run using the Emission1 distribution and MERRA2 reanalysis meteorology are shown for reference (solid light blue and green lines). Also, lines colored blue represent simulations using the emission record derived from the 3-box model analysis of observations while all green lines indicate simulations with emissions kept constant after 2012 at the 2012 rate. **a-c**, Results from CAM as a function of emission distribution (E1 and E3) and nudging methodology (temperature and winds, or wind-only (UV nudged)). **d-f**, Results from WACCM as a function of reanalysis meteorology (MERRA1 or MERRA2). **g-i**, Results from WACCM with GEOS5 reanalysis meteorology and two different emission distributions (E2 and E1). The comparisons are made for the CFC-11 global rate of change at Earths' surface (**a,d,g**; left column), the surface mean hemispheric difference (**b,e,h**; middle column), and the change in the surface mean hemispheric difference relative to the mean during 2010-2012 (**c,f,l**; right column; note expanded time axis). All quantities being compared are derived from hemispheric means determined from cosine of latitude weighting of observed or simulated mole fractions at sampling locations (Methods).

Extended Data Figure 9| The sensitivity of derived bank release rates to CFC-11 lifetime and incineration. Black squares and dashed blue line are repeated from Fig. 2 and are derived with a 57.5 year lifetime. Considering the same reported production history and emission histories derived for the likely range of CFC-11 lifetimes (43 – 67 y; 1) are given as red lines. Including quantities of CFC-11 destroyed (e.g., incineration) reported to UNEP (grey circles) affect this result minimally.

Extended Data Item references:

(1) Hamilton, K. & Fan, S.-M. Effects of the stratospheric quasi-biennial oscillation on long-lived greenhouse gases in the troposphere, *J. Geophys. Res*. **105** 20581-20587 (2000).

(2) Simmonds, P. G. *et al*. Interannual fluctuations in the seasonal cycle of nitrous oxide and chlorofluorocarbons due to the Brewer-Dobson circulation. *J. Geophys. Res*. **118**, 10694-10706 (2013) 10.1002/jgrd.50832.

(3) Nevison, C.D., *et al*. Exploring causes of interannual variability in the seasonal cycles of tropospheric nitrous oxide. *Atmos. Chem. Phys*. **11**, 3713-3730 (2011) 10.5194/acp-11-3713-2011.

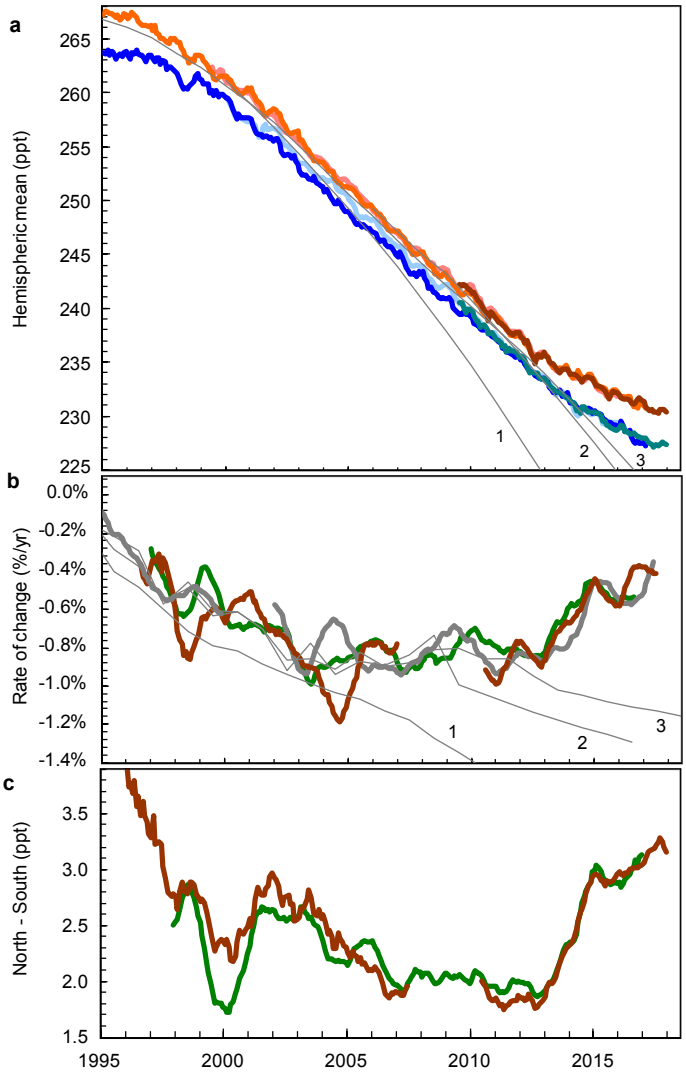
a
Hemispheric mean (ppt)
265
260
255
250
245
240
235
230
225
1
2
3
b
Rate of change (%/yr)
0.0%
-0.2%
-0.4%
-0.6%
-0.8%
-1.0%
-1.2%
-1.4%
1
2
3
c
North - South (ppt)
3.5
3.0
2.5
2.0
1.5
1995
2000
2005
2010
2015

Figure 1

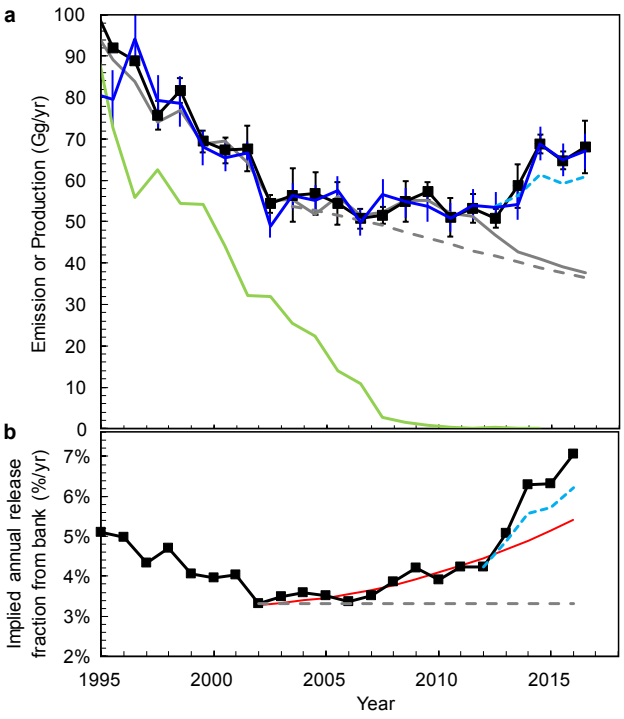
a
b
Emission or Production (Gg/yr)
Implied annual release fraction from bank (%/yr)
Year
100
90
80
70
60
50
40
30
20
10
0
7%
6%
5%
4%
3%
2%
1995
2000
2005
2010
2015

Figure 2

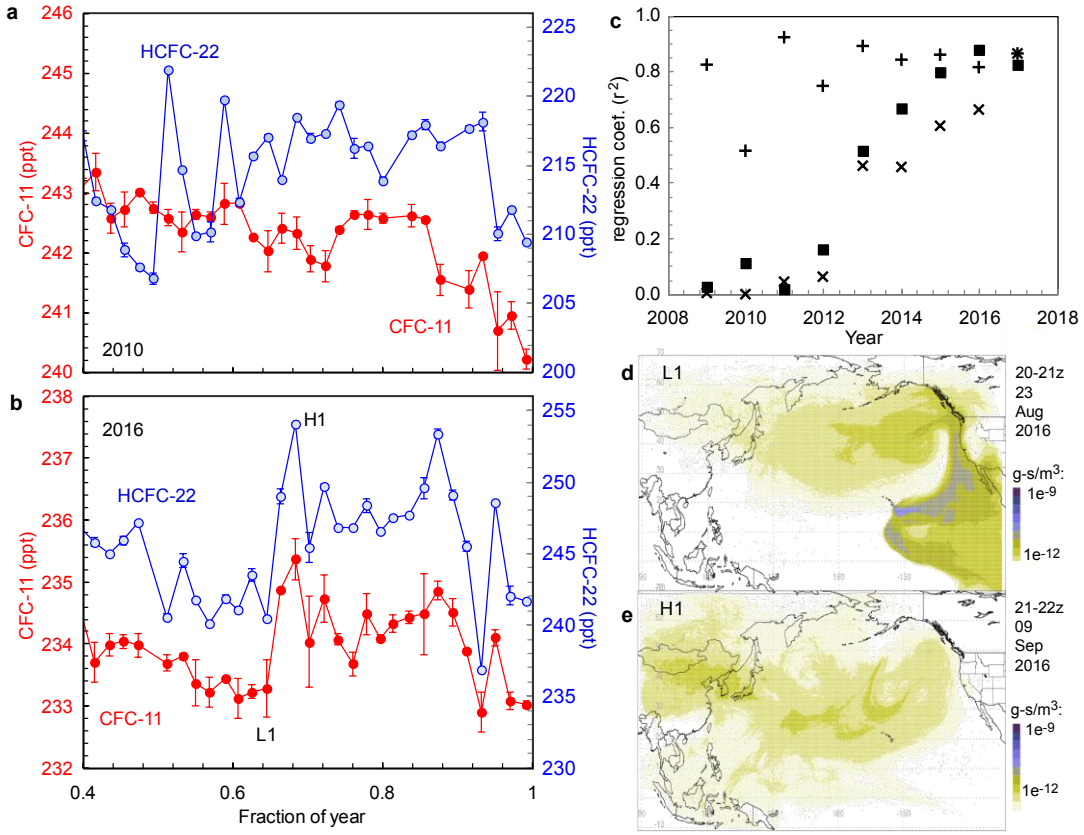
a
HCFC-22
CFC-11
2010
CFC-11 (ppt)
HCFC-22 (ppt)
b
2016
H1
HCFC-22
CFC-11
L1
Fraction of year
c
regression coef. (r^2)
Year
d
L1
20-21z
23
Aug
2016
g-s/m3:
1e-9
1e-12
e
H1
21-22z
09
Sep
2016
g-s/m3:
1e-9
1e-12

Figure 3

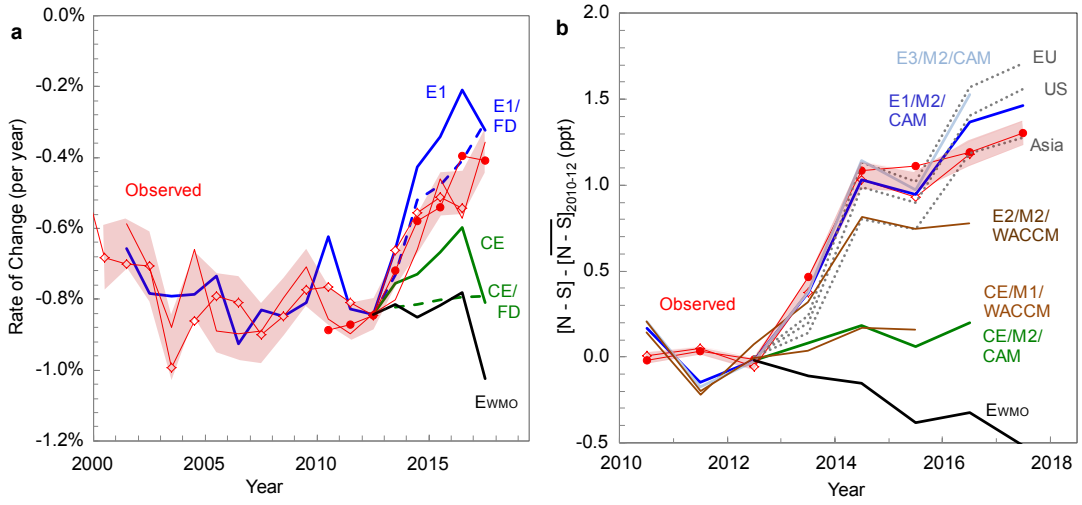
a
0.0%
-0.2%
-0.4%
-0.6%
-0.8%
-1.0%
-1.2%
Rate of Change (per year)
2000
2005
2010
2015
Year
Observed
E1
E1/
FD
CE
CE/
FD
EWMO
b
2.0
1.5
1.0
0.5
0.0
-0.5
[N - S] - [N - S]2010-12 (ppt)
2010
2012
2014
2016
2018
Year
E3/M2/CAM
EU
US
E1/M2/
CAM
Asia
E2/M2/
WACCM
Observed
CE/M1/
WACCM
CE/M2/
CAM
EWMO

Figure 4

Year	*Emis. 3-box*	*1 s.d.*	*Emis. 12-box*	*Low*	*High*	*Production **
1994	103.9	4.6	81.2	7.5	6.1	99.8
1995	92.0	4.5	79.5	6.3	7.0	72.6
1996	89.0	4.3	94.3	5.6	6.3	55.9
1997	75.8	3.5	79.4	6.6	6.1	62.5
1998	81.7	3.0	78.5	5.6	6.6	54.3
1999	69.5	2.6	68.1	4.4	3.9	54.1
2000	67.3	3.1	65.5	3.3	3.7	44.1
2001	67.7	5.6	66.7	3.0	2.6	32.2
2002	54.4	2.1	48.9	2.7	3.0	31.8
2003	56.5	6.5	56.4	3.4	2.9	25.5
2004	56.9	5.1	55.2	3.6	3.7	22.3
2005	54.4	5.1	57.6	3.3	3.5	13.9
2006	50.8	2.4	49.9	3.3	3.2	10.9
2007	51.6	2.0	56.6	2.9	3.6	2.8
2008	54.9	5.0	54.9	3.9	3.2	1.4
2009	57.4	2.2	53.7	3.6	4.1	0.9
2010	51.1	4.7	50.9	3.4	3.7	0.4
2011	53.2	3.5	53.9	3.4	3.9	0.1
2012	50.9	2.3	53.4	3.6	3.7	0.3
2013	58.7	5.3	54.3	3.8	3.7	0.0
2014	68.9	2.3	68.8	3.9	4.1	0.1
2015	64.8	2.2	64.9	3.8	3.9	--
2016	68.0	6.4	67.2	4.5	4.1	--

All values in Gg/y.

* Total CFC-11 production reported to the UNEP Ozone Secretariat. The Montreal Protocol requires that all CFC production be reported to the Ozone Secretariat, including production for dispersive and non-dispersive uses, production for use as chemical intermediates or feedstocks, and any unintentional by-production. No subtractions for reported destruction amounts are included in these values; cumulative destruction of CFC-11 reported to the Ozone Secretariat totaled 16 Gg in all years since 1998 (4).

Extended Data Table 1

a

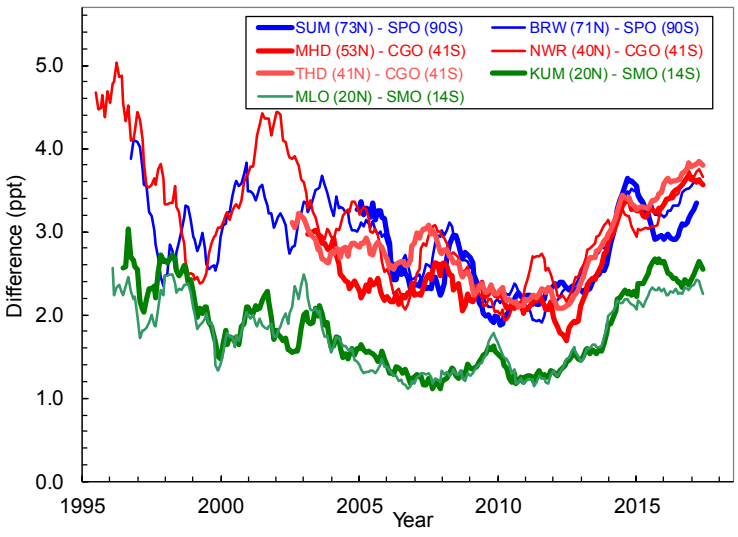

b

Site	*Code*	*Latitude*	*Longitude*	*Altitude* (m)*	*Methods***
South Pole, Antarctica	SPO	90°S		2837	I, F
Palmer Station, Antarctica	PSA	64.6°S	64.0°W	15	F
Cape Grim, Australia	CGO	40.682°S	144.688°E	164	F
American Samoa	SMO	14.247°S	170.564°W	77	I,F
Mauna Loa, USA	MLO	19.5362°N	155.5763°W	3433	I,F
Cape Kumukahi, USA	KUM	19.516°N	154.811°W	39	F
Niwot Ridge, USA	NWR	40.0518°N	105.5854°W	3523	I,F
Trinidad Head, USA	THD	41.054°N	124.151°W	120	F
Mace Head, Ireland	MHD	53.3°N	9.9°W	42	F
Barrow, USA	BRW	71.323°N	156.611°W	27	I,F
Alert, Canada	ALT	82.5°N	62.3°W	210	F
Summit, Greenland	SUM	72.6°N	38.4°W	3209	I,F

* altitudes represent the sample inlet location, in meters above sea level.
** I = GCECD in-situ instrument making ongoing measurements multiple times per day.
F = from flasks collected approximately weekly that are measured at the NOAA labs in Boulder by GCECD and GCMS.

Extended Data Figure 1

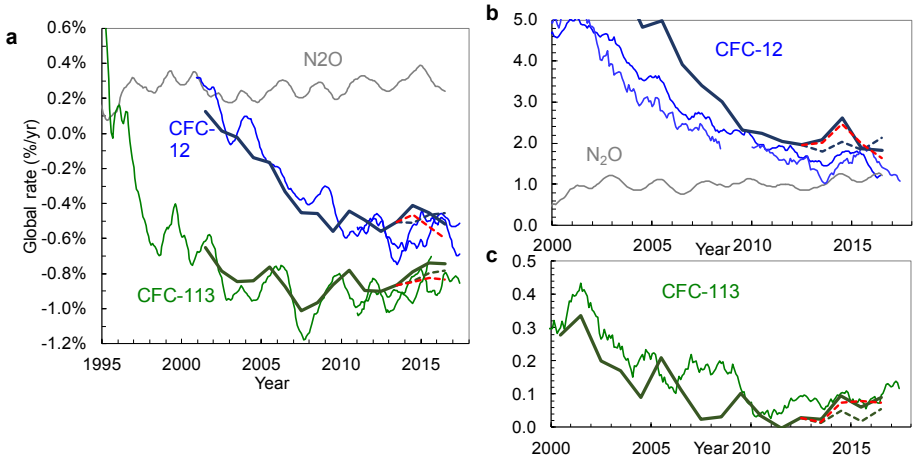

Extended Data Figure 2

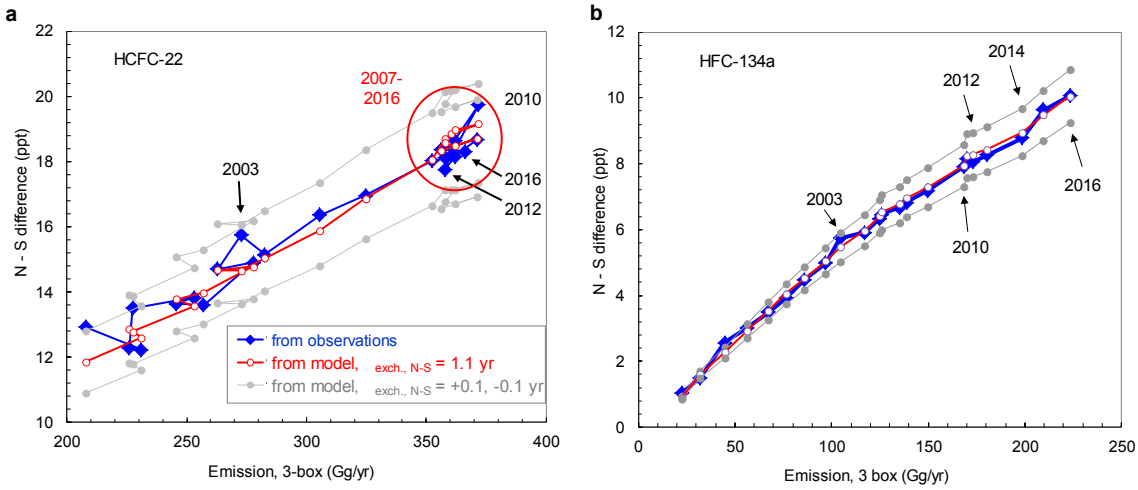

Extended Data Figure 3

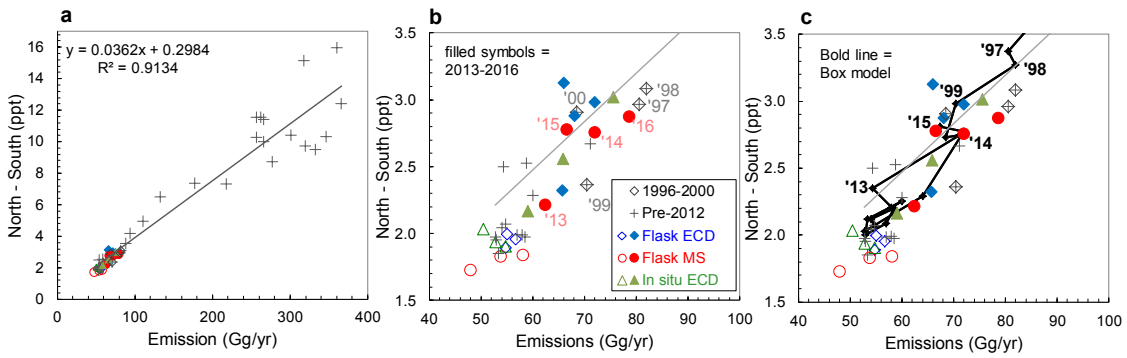

Extended Data Figure 4

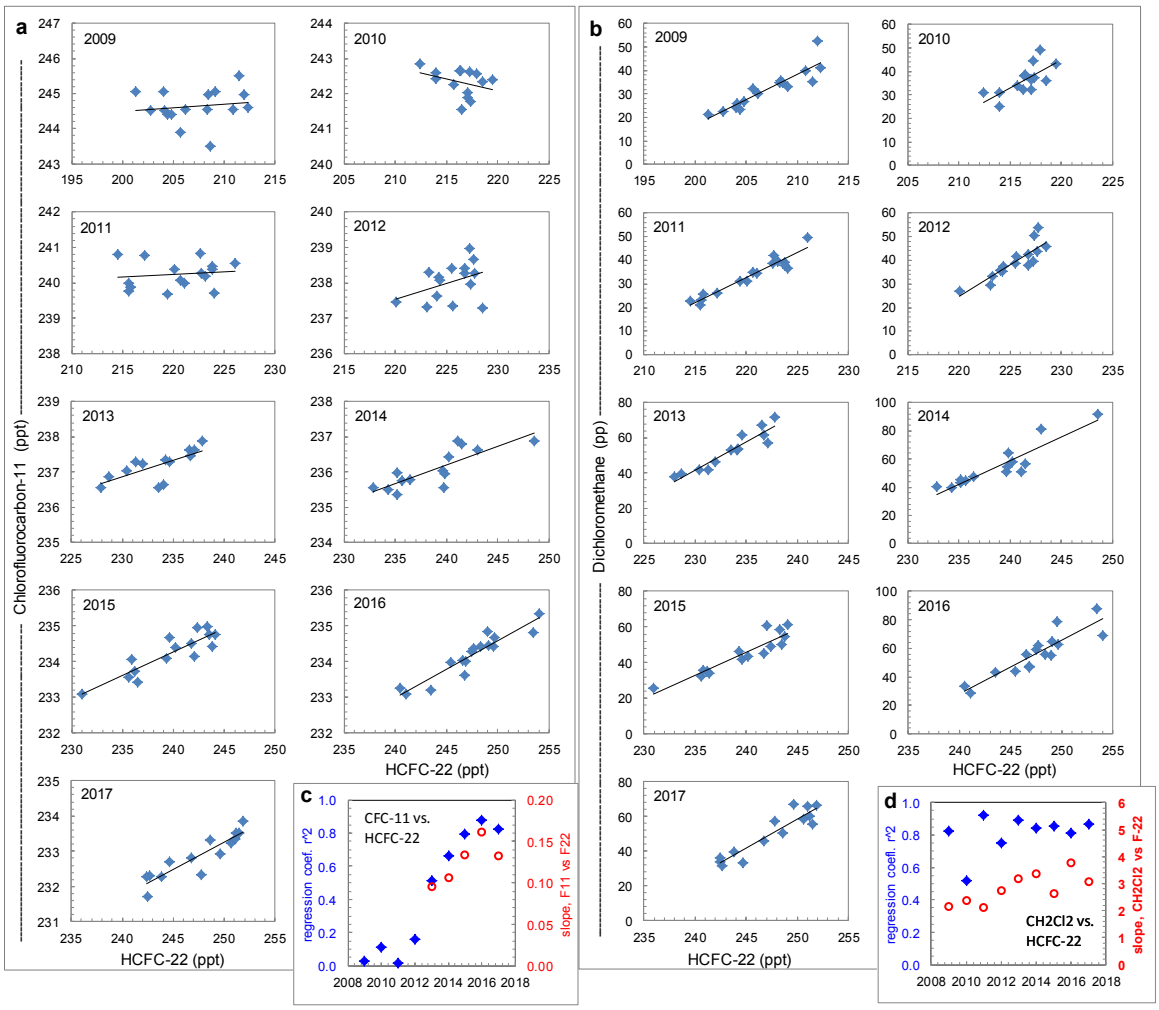

Extended Data Figure 5

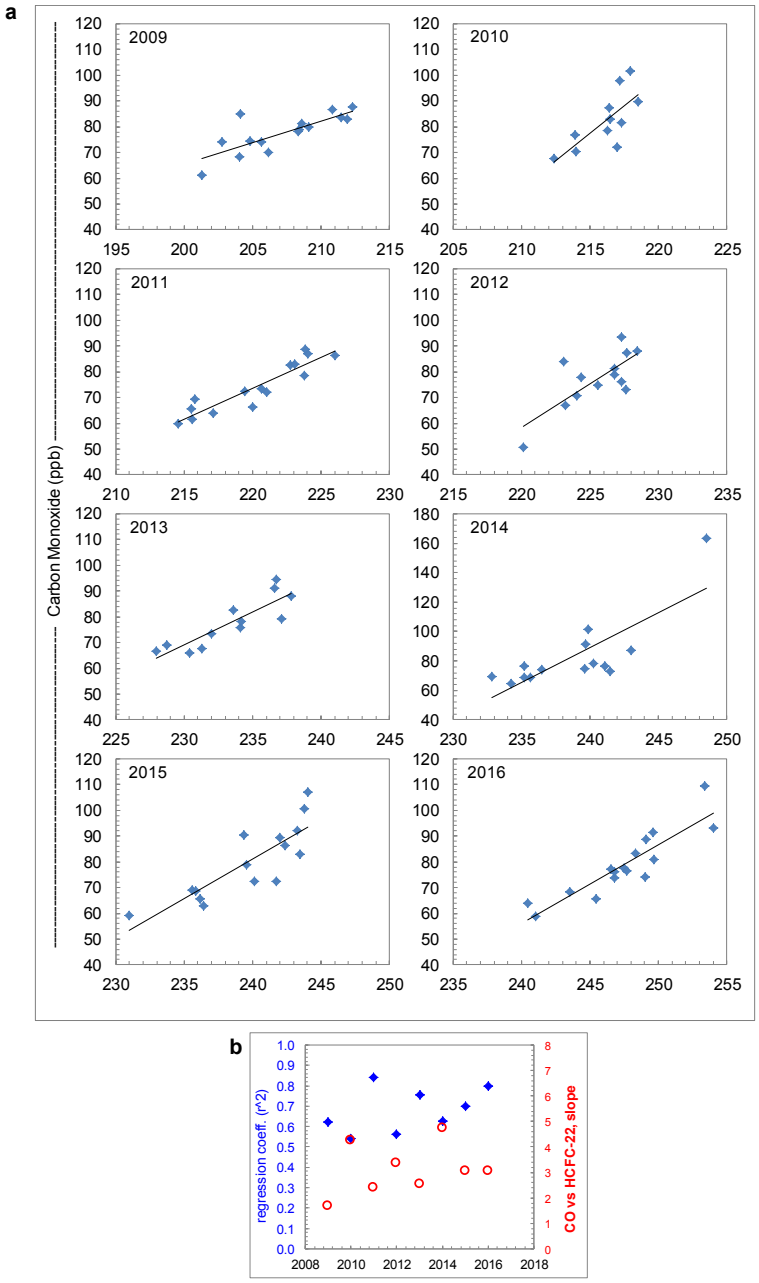

Extended Data Figure 6

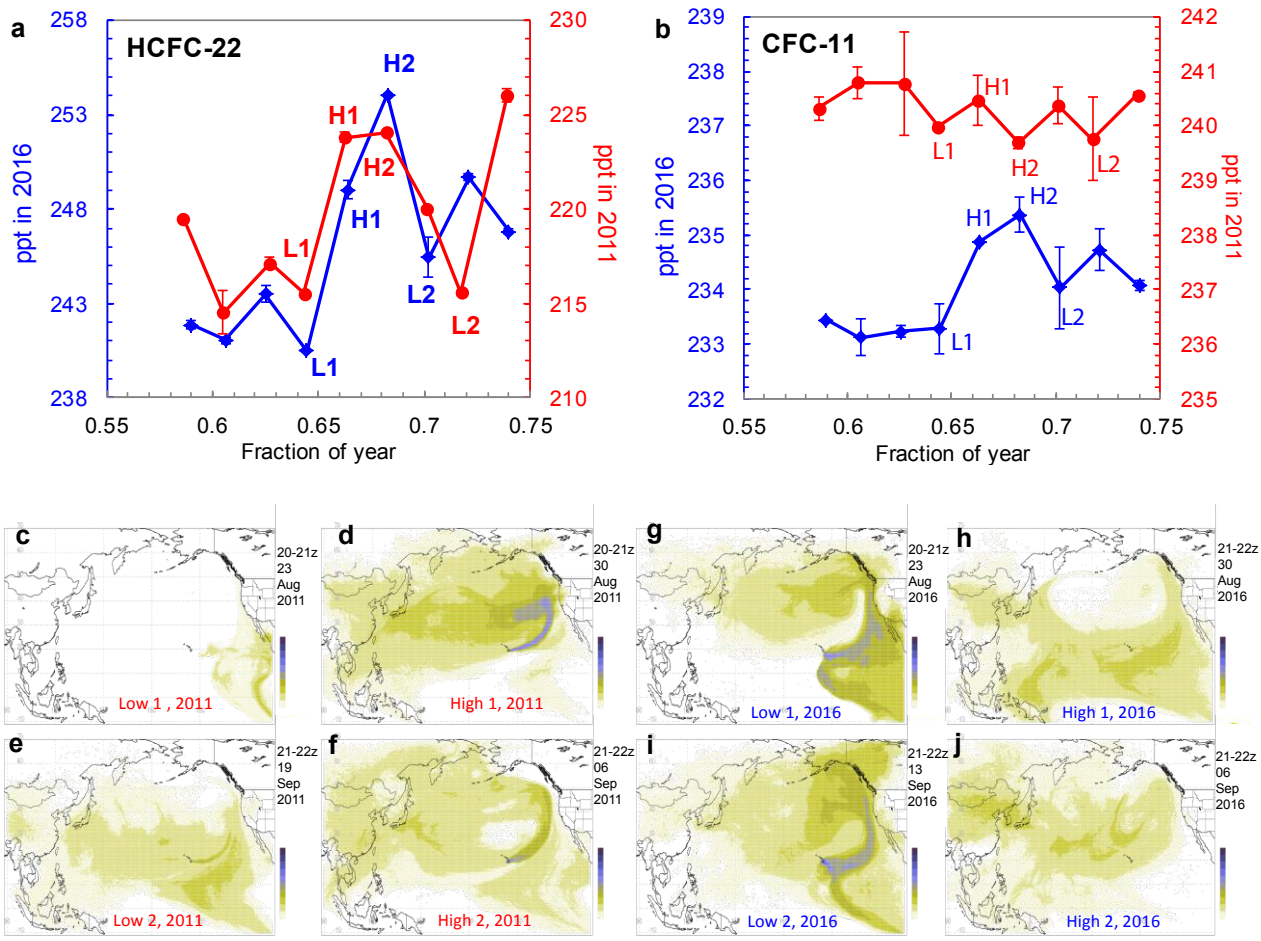

Extended Data Figure 7

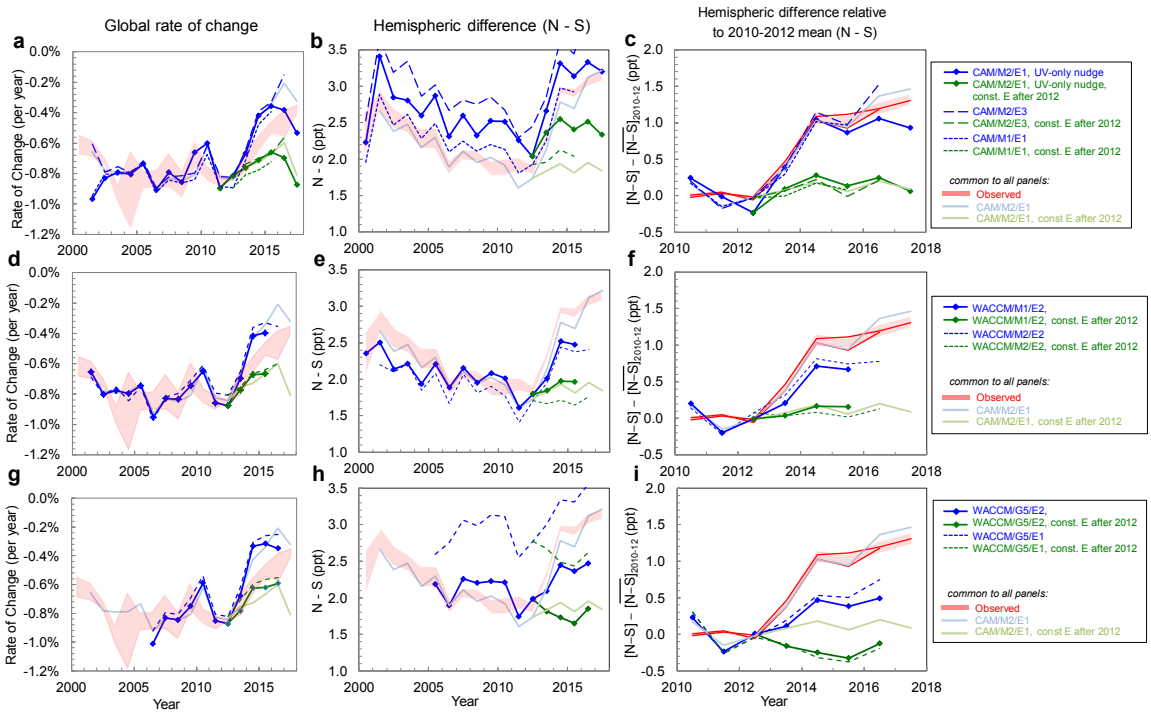

Extended Data Figure 8

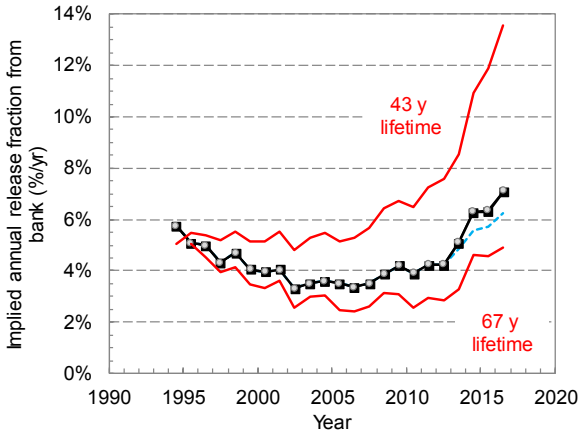

Extended Data Figure 9